

Title page

Classification: PHYSICAL SCIENCE: Physics

Title: Superconductive “sodalite”-like clathrate calcium hydride at high pressures

Author affiliation: Hui Wang¹, John S. Tse², Kaori Tanaka², Toshiaki Iitaka³, and Yanming Ma^{1*}

¹State Key Lab of Superhard Materials, Jilin University, Changchun 130012, P. R. China,

²Department of Physics and Engineering Physics, University of Saskatchewan, Saskatoon,
Saskatchewan, S7N 5E2, Canada,

³Computational Astrophysics Laboratory, RIKEN, 2-1 Hirosawa, Wako, Saitama 351-0198, Japan.

***Corresponding author:**

Yanming Ma

State Key Lab of Superhard Materials, Jilin University, Changchun 130012, China

TEL: +86-431-85168276

FAX: +86-431-85168276

EMAIL: mym@jlu.edu.cn

Manuscript information: 9 text pages and 4 figures

Abbreviations: Calcium hydride | High pressure | sodalite structure

Abstract

Hydrogen-rich compounds hold promise as high-temperature superconductors under high pressures. Recent theoretical hydride structures on achieving high-pressure superconductivity are composed mainly of H₂ fragments. Through a systematic investigation of Ca hydrides with different hydrogen contents using particle-swarm optimization structural search, we show that in the stoichiometry CaH₆ a body-centred cubic structure with hydrogen that forms unusual “sodalite” cages containing enclathrated Ca stabilizes above pressure 150 GPa. The stability of this structure is derived from the acceptance by two H₂ of electrons donated by Ca forming a “H₄” unit as the building block in the construction of the 3-dimensional sodalite cage. This unique structure has a partial occupation of the degenerated orbitals at the zone centre. The resultant dynamic Jahn–Teller effect helps to enhance electron–phonon coupling and leads to superconductivity of CaH₆. A superconducting critical temperature (T_c) of 220–235 K at 150 GPa obtained from the solution of the Eliashberg equations is the highest among all hydrides studied thus far.

\body

Introduction

Current studies of the hydrides of simple elements at high pressures are motivated by the proposition that a high T_c may be achieved from “pre-compressed” H_2 in dense hydrogen-dominant hydrides¹. Superconductivity has been reported in SiH_4 ², although controversy surrounds models of the origin of superconductivity and the structure of the superconducting state³⁻⁵. Many theoretical structures have the predicted T_c values ranging from 10 to 139 K⁶⁻¹². Except for AlH_3 ¹³, in which superconductivity was predicted but not observed, a common feature of these structures is the ubiquitous presence of molecular hydrogen fragments. At high pressures, unfavourable electron–electron repulsion in the atomic valence shells can be reduced by migration and localization in the empty interstitial regions^{14,15}. Introduction of an electronegative element, as was demonstrated in the case of K-Ag¹⁶, increases the ability of the electronegative Ag atoms to accommodate electrons from K into the outermost $5s$ and $5p$ valence shells, thereby forming a bonding network and stabilizing the new alloy structures that otherwise would not be observed under ambient pressures. Recently, Zurek *et al.*^{17,18} demonstrated that charge transfer from lithium or sodium to hydrogen molecules under high pressures could lead to the formation of new metallic lithium- or sodium-hydride alloys. Depending on the stoichiometry, the structures consisting of “pre-dissociated” molecular H_2 and/or monoatomic hydrogen.

Results and Discussion

The known calcium hydrides have a stoichiometry of CaH_2 at ambient pressures. Here, we explored other calcium hydrides with larger hydrogen contents by compressing a mixture containing Ca + hydrogen or CaH_2 + hydrogen. The search for stable CaH_{2n} ($n = 2 - 6$) structures at high pressures was performed using the particle-swarm optimization structure prediction algorithm¹⁹ in combination with *ab initio* calculations. For each stoichiometry, calculations were performed at pressures 50-200 GPa with up to four formula units in the model. The enthalpies of candidate structures relative to the products of dissociation into CaH_2 + solid H_2 at the

appropriate pressures are summarized in Fig. 1(a). The essential information can be summarized as follows: (i) except for CaH₁₀, stable structures began to emerge at pressures < 50 GPa; (ii) CaH₄ was the most stable phase at pressures between 50 and 150 GPa, while at 200 GPa CaH₆ had the lowest enthalpy of formation; (iii) the breakup of hydrogen molecules depended on the Ca/H ratio, and a higher susceptibility to dissociation was observed at higher ratios. Notably, calcium hydrides with stoichiometry having odd number of hydrogen (e.g. CaH₃, CaH₅, and CaH₇, etc) were found to be energetically very unfavourable and were excluded in the discussions (see Supplementary Information).

The structures of the stable phases for each stoichiometry at 150 GPa are shown in Fig. 1(b)-(d). Three types of hydrogen species, “H₄” units, monatomic H + H₂, and molecular H₂, were observed. CaH₄ had a tetragonal (*I4/mmm*, Pearson symbol tI10) structure and included a body-centred arrangement of Ca and two molecular and four monatomic hydrogen units (Ca₂(H₂)₂(H)₄). The structure of CaH₆ adopted a remarkable cubic form (*Im* $\bar{3}$ *m*, Pearson symbol cI14), with body-centred Ca atoms and, on each face, squared “H₄” units tilted 45° with respect to the plane of the Ca atoms. These “H₄” units were interlinked to form a sodalite framework with a Ca atom enclathrated at the centre of each cage. The next stable polymorph, CaH₁₂, had a rhombohedral (*R* $\bar{3}$, Pearson symbol hR13) structure consisting entirely of molecular H₂.

The presence of different types of hydrogen can be rationalized based on the effective number of electrons contributed by the Ca atom and accepted by each H₂ molecule. Assuming that the two valence electrons of each Ca atom were completely “ionized” and accepted by H₂ molecules, the “formal” effectively added electron (EAE) per H₂ for CaH₄ was 1e/H₂, for CaH₆ was (2/3)e/H₂, and was (1/3)e/H₂ for CaH₁₂. Because H₂ already had a filled σ bond, the added electrons resided in the antibonding σ^* orbitals, which weakened the H-H bond (i.e., lengthened the H-H bond length) and

eventually resulted in complete dissociation. The presence of H and H₂ units in the CaH_{2n} structures depended on the number of EAEs. Two formulae were present in each unit cell of CaH₄. Because half (two) of each H₂ molecule was retained, the remaining two H₂ molecules had to accommodate four “excess” electrons into their σ^* orbital, which broke up the molecules into monatomic hydrides (H⁻). The formation of “H₄” units in CaH₆ was not accidental. If molecular hydrogen atoms were present, each σ^* orbital of H₂ had to accommodate $(2/3)e$. This led to a physically unfavourable structure with significant weakening of the intramolecular H-H bonds. There is, however, an alternative lower energy structure, the one predicted here. From molecular orbital theory, a square “H₄” unit should possess a half-filled degenerated “non-bonding” orbital (Fig. 2a). This orbital, in principle, can accommodate up to two electrons without detrimentally weakening the H-H bond (Fig. 2b). It should be noted that at 150 GPa, the H...H distance of “H₄” in the cI14 structure of CaH₆ was 1.24 Å, which was substantially shorter than both the monoatomic H...H distance of 1.95 Å and the H...H₂ distance of 1.61 Å in CaH₄, but in good agreement with those of 1.27 and 1.17 Å in isolated H₄²⁻ and “H₄” squares, respectively. This suggested the presence of a weak covalent H...H interaction in CaH₆. As will be described below, the “H₄” unit is the fundamental building block of the sodalite cage.

In CaH₁₂, the EAE was $(1/3)e/H_2$, which could be taken up by H₂ without severing the bond. Extending this concept further then predicted that CaH₁₂ and hydride-alloys with a high H content (smaller EAE) would be composed predominantly of molecular H₂. An important observation in support of the EAE description given above is that the H-H bond in CaH₄ lengthened from 0.81 Å at 100 GPa to 0.82 Å at 150 GPa, while the H-H bond in CaH₁₂ shortened from 0.81 Å to 0.80 Å. Here, more Ca valence electrons in CaH₄ were available for transfer to the H₂ σ^* orbitals than were available in CaH₁₂, thereby more severely weakening the bond in CaH₄. This effect was relatively small for CaH₁₂, in which the H-H bond was shortened due to compression.

The zero-point motion was not included in the calculation of the formation enthalpy of the various hydrides (Fig. 1a), although it is expected to be very influential due to the presence of large amounts of hydrogen. We estimated the zero-point energies of CaH₆ and CaH₄ using the quasiharmonic model²⁰ at 150 GPa. It was found that the inclusion of zero-point motion significantly lowered the formation enthalpy of CaH₆ with respect to CaH₄ (Supplementary Figure S11). As a consequence, CaH₆ became more stable at and above 150 GPa. The physical mechanism underlying this effect stemmed from the “H₄” moieties, which included much longer H-H distances and led to significantly softened phonons. This contrasted with other Ca hydrides studied (e.g., CaH₄ and CaH₁₂), in which the presence of “H₂” molecular units gave rise to higher frequency phonons and, thus, a larger zero-point energy.

The three-dimensional sodalite cage in CaH₆ is the result of interlink of other “H₄” units via each H atom at the corner of one “H₄” unit. So, what is the electronic factor promoting the formation of these “H₄” units? To answer this question, the electron localization functions (ELF) of a hypothetical bare bcc Ca lattice with the H atoms removed and CaH₆ hydride (Fig. 3a and 3b) were examined. In bare bcc Ca, regions with ELF values of 0.58 were found to localize at the H atom sites in the “H₄” units on the faces of the cube. The ELF of CaH₆ hydride suggested that no bonds were present between the Ca and H. A weak “pairing” covalent interaction with an ELF of 0.61, however, was found between the H atoms that formed a square “H₄” lattice. Their formation resulted from the accommodation by H₂ of “excess” electrons from the Ca. An electron topological analysis also showed the presence of a bond-critical point²¹ along the path connecting neighbouring H atoms. The integrated charge within the H atomic basin was 1.17*e*, which corresponded to a charge transfer of 1.02*e* from each Ca. A partially “ionized” Ca was also clearly supported by the band structure and the density of states as reported in Fig. 3c and Supplementary Fig. S15. At 150 GPa, Ca underwent an *s-d* hybridization with an electron transferred from the 4*s* to the 3*d*

orbital. In CaH_6 , the Ca site symmetry was $m\bar{3}m (O_h)$ and the Ca $3d$ manifold was clearly split into the e_g and t_{2g} bands, with the lower energy e_g band partially occupied.

A comparison of the band structures of CaH_6 , “ H_6 ” (Ca_0H_6), and bare Ca (CaH_0) provided additional supporting evidence. Even without the presence of Ca, the valence band width of the hypothetical “ H_6 ” (Fig. 3d) was 15.2 eV, comparable to 16.4 eV for CaH_6 (Fig. 3c). In comparison, the valence band width of the “bare” bcc Ca was only 4.3 eV (Fig. 3e). The band structure of CaH_6 near the Fermi level was modified from “ H_6 ” due to the hybridization between Ca $3d$ and H $1s$ orbital; however, the trend in the electronic band dispersions from -2 to -16.4 eV was remarkably similar to that of “ H_6 ” from 3 to -15.2 eV.

Sodalite cage was constructed from linking of “ H_4 ” units and this topologically resulted in the formation of “ H_6 ” faces. In fact, a primitive cell of CaH_6 can be seen as composed of a “ H_6 ” hexagon and a Ca. Band structure analysis suggested that four conduction bands of “ Ca_0H_6 ” sodalite cage (Fig. 3d) were half-filled and the addition of maximal two electrons to “ H_6 ” gave rise to partial occupancy of the degenerate bands at Γ as indicated in CaH_6 (Fig. 3c). Partial occupancy of a degenerate orbital results in an orbitally degenerate state and is subject to Jahn–Teller (JT) distortion (Fig. 2)²². The JT effect involves coupling between the electron and nuclear degrees of freedom, leading to distortions in the structure, and it lifts the orbital degeneracy. If the distortion is dynamic, JT vibrations can contribute to superconductivity. The same mechanism has been invoked to explain the superconductivity in B-doped diamond²³. To investigate this possibility, electron–phonon coupling (EPC) calculations on the sodalite structure of CaH_6 at 150 GPa were performed. The phonon dispersion curves, phonon linewidth $\gamma(\omega)$, EPC parameter λ , and Eliashberg spectral function $\alpha^2F(\omega)$ were calculated. A gap at 430 cm^{-1} (Fig. 4) separated the phonon spectrum into two regions: the lower frequency branches were associated with the motions of both Ca

and H, whereas the higher frequency branches were mainly associated with H atoms. The combined contribution (19% and 81%, respectively) gave an EPC parameter λ of 2.69. The calculated phonon linewidths (Fig. 4) showed that the EPC was derived primarily from the T_{2g} and E_g modes at the zone centre Γ . Incidentally, these two bands, respectively, were the in-plane breathing and rocking vibrations of the H atoms belonging to the “H₄” unit. The corresponding atomic vibrations led to distortions in the square planar structure. Moreover, both phonon branches showed significant phonon softening along all symmetric directions. A large EPC also benefited from the high density of states at the Fermi level caused by a Van Hove singularity at Γ (Fig. 3c). The very large EPC was unprecedented for the main group hydrides. Previous calculations on a variety of systems predicted an EPC in the range of 0.5–1.6¹¹. The mechanism suggested here is not inconsistent with the mechanisms found in JT-induced superconductivity in alkali intercalated C₆₀, in which the intramolecular vibrations are responsible for distortions that lower the symmetry of the molecules, which is favourable for electron–phonon processes^{24,25}.

T_c was calculated based on the spectral function $\alpha^2F(\omega)$ by numerically solving the Eliashberg equations²⁶, which consist of coupled non-linear equations describing the frequency-dependent order parameter and renormalisation factor. The Coulomb repulsion is taken into account in terms of the Coulomb pseudopotential, μ^* , scaled to a cutoff frequency (typically six times the maximum phonon frequency)²⁷. At 150 GPa, the predicted T_c values were 235 K and 220 K using typical values for μ^* of 0.1 and 0.13, respectively. EPC calculations were also performed for 200 GPa and 250 GPa, in which the calculated T_c was found to decrease with pressure (201 K at 200 GPa and 187 K at 250 GPa for $\mu^*= 0.13$), with a pressure coefficient (dT_c/dP) of -0.33 K/GPa. T_c of the order of 200 K is among the highest for all reported hydrides.

The predicted high T_c for CaH₆ is very encouraging, but it must be viewed with caution. Formally, there is no upper limit to the value of T_c within the

Midgal–Eliashberg theory of superconductivity. Two practical factors must be considered. The calculation of the EPC is based on the harmonic approximation and without consideration of electron correlation effects. Because strong electron–phonon coupling in CaH₆ arises from the proximity of the electronic and structural instabilities, anharmonicity of the atomic motions can lead to renormalization of the vibrational modes, as demonstrated in a study of AlH₃. In that study, lower renormalized frequencies were found to reduce the EPC and suppress superconductivity²⁸. On the other hand, the electron–phonon matrix elements may be enhanced by anharmonic vibrations, as in the case of disordered materials²⁹. In a recent hybrid functional study of C₆₀ anions, the inclusion of Hartree–Fock exchange contributions was shown to have little effect on the structural properties and phonon frequencies, but resulted in a strong increase in the electron–phonon coupling²⁴.

The formation of a hydrogen sodalite cage with enclathrated calcium in CaH₆, reported here for hydrogen-rich compounds, provides an unexpected example of a good superconductor created by the compression of a mixture of elemental calcium + hydrogen or CaH₂ + hydrogen. This novel superconductor can also be viewed as consisting of unique square “H₄” units and electron-donating calcium atoms subject to JT effects. Dense superconductive states, such as those reported here, may be favoured in other mixtures of elemental metals + hydrogen or any hydride + hydrogen upon compression. This work highlights the major role played by pressure in effectively overcoming the kinetic barrier to formation in the synthesis of novel hydrides.

Methods

Our structure prediction approach is based on a global minimization of free energy surfaces merging *ab initio* total-energy calculations via particle swarm optimization technique as implemented in CALYPSO (Crystal structure AnaLYsis by Particle Swarm Optimization) code¹⁹. Our CALYPSO method unbiased by any known structural information has been benchmarked on various known systems¹⁹ with

various chemical bondings and had several successful prediction of high pressure structures of Li, Mg, and Bi_2Te_3 ³⁰⁻³², among which the insulating orthorhombic (*Aba2*, Pearson symbol oC40) structure of Li and the two low-pressure monoclinic structures of Bi_2Te_3 have been confirmed by independent experiments^{32,33}. The underlying *ab initio* structural relaxations were carried out using density functional theory within the Perdew-Burke-Ernzerhof exchange-correlation³⁴ as implemented in the VASP code³⁵. The all-electron projector-augmented wave method³⁶ was adopted with $1s$ and $3p^64s^2$ treated as valence electrons for H and Ca, respectively. Electronic properties, lattice dynamics and electron-phonon coupling were studied by density functional (linear-response) theory as implemented in the QUANTUM ESPRESSO package³⁷. More computational details can be found in the supplementary information.

References

1. Ashcroft, N. W. Hydrogen Dominant Metallic Alloys: High Temperature Superconductors? *Phys. Rev. Lett.* **92**, 187002 (2004).
2. Eremets, M. I., Trojan, I. A., Medvedev, S. A., Tse, J. S. & Yao, Y. Superconductivity in Hydrogen Dominant Materials: Silane. *Science* **319**, 1506-1509 (2008).
3. Degtyareva, O., Proctor, J. E., Guillaume, C. L., Gregoryanz, E. & Hanfland, M. Formation of transition metal hydrides at high pressures. *Solid State Commun.* **149**, 1583-1586 (2009).
4. Hanfland, M., Proctor, J. E., Guillaume, C. L., Degtyareva, O. & Gregoryanz, E. High-Pressure Synthesis, Amorphization, and Decomposition of Silane. *Phys. Rev. Lett.* **106**, 095503 (2011).
5. Strobel, T. A. *et al.* High-pressure study of silane to 150 GPa. *Phys. Rev. B* **83**, 144102 (2011).
6. Feng, J. *et al.* Structures and Potential Superconductivity in SiH_4 at High Pressure: En Route to "Metallic Hydrogen". *Phys. Rev. Lett.* **96**, 017006 (2006).
7. Tse, J. S., Yao, Y. & Tanaka, K. Novel Superconductivity in Metallic SnH_4 under High Pressure. *Phys. Rev. Lett.* **98**, 117004 (2007).
8. Gao, G. *et al.* Superconducting High Pressure Phase of Germane. *Phys. Rev. Lett.* **101**, 107002 (2008).
9. Martinez-Canales, M. *et al.* Novel Structures and Superconductivity of Silane under Pressure. *Phys. Rev. Lett.* **102**, 087005 (2009).
10. Kim, D. Y., Scheicher, R. H., Mao, H.-K., Kang, T. W. & Ahuja, R. General trend for pressurized superconducting hydrogen-dense materials. *Proc. Natl. Acad. Sci. U.S.A.* **107**, 2793-2796 (2010).
11. Li, Y. *et al.* Superconductivity at ~ 100 K in dense $\text{SiH}_4(\text{H}_2)_2$ predicted by first principles. *Proc. Natl. Acad. Sci. U.S.A.* **107**, 15708-15711 (2010).
12. Jin, X. *et al.* Superconducting high-pressure phases of disilane. *Proc. Natl. Acad. Sci. U.S.A.* **107**, 9969-9973 (2010).
13. Goncharenko, I. *et al.* Pressure-Induced Hydrogen-Dominant Metallic State in Aluminum Hydride. *Phys. Rev. Lett.* **100**, 045504 (2008).
14. Neaton, J. B. & Ashcroft, N. W. Pairing in dense lithium. *Nature* **400**, 141-144 (1999).
15. Tamblyn, I., Raty, J.-Y. & Bonev, S. A. Tetrahedral Clustering in Molten Lithium under Pressure. *Phys. Rev. Lett.* **101**, 075703 (2008).
16. Tse, J. S. Crystallography of selected high pressure elemental solids. *Zeitschrift für Kristallographie* **220**, 521-530 (2005).
17. Zurek, E., Hoffmann, R., Ashcroft, N. W., Oganov, A. R. & Lyakhov, A. O. A little bit of lithium does a lot for hydrogen. *Proc. Natl. Acad. Sci. U.S.A.* **106**, 17640-17643 (2009).
18. Baettig, P. & Zurek, E. Pressure-Stabilized Sodium Polyhydrides: NaH_n ($n > 1$). *Phys. Rev. Lett.* **106**, 237002 (2011).
19. Wang, Y., Lv, J., Zhu, L. & Ma, Y. Crystal structure prediction via particle-swarm optimization.

- Physical Review B* **82**, 094116 (2010).
20. Ma, Y. & Tse, J. S. Ab initio determination of crystal lattice constants and thermal expansion for germanium isotopes. *Solid State Commun.* **143**, 161-165 (2007).
 21. Richard, F. W. B. *Atoms in molecules: a quantum theory.* (Clarendon Press, 1990).
 22. Jahn, H. A. & Teller, E. Stability of Polyatomic Molecules in Degenerate Electronic States. I. Orbital Degeneracy. *Proc. Roy. Soc. A* **161**, 220-235 (1937).
 23. Ma, Y. *et al.* First-principles study of electron-phonon coupling in hole- and electron-doped diamonds in the virtual crystal approximation. *Phys. Rev. B* **72**, 014306 (2005).
 24. Laflamme Janssen, J., Côté, M., Louie, S. G. & Cohen, M. L. Electron-phonon coupling in C₆₀ using hybrid functionals. *Phys. Rev. B* **81**, 073106 (2010).
 25. Schlüter, M., Lannoo, M., Needels, M., Baraff, G. A. & Tománek, D. Superconductivity in alkali intercalated C₆₀. *J. Phys. Chem. Solids* **53**, 1473-1485 (1992).
 26. Eliashberg, G. M. Interactions between electrons and lattice vibrations in a superconductor. *Sov. Phys. JETP* **11**, 696 (1960).
 27. Yao, Y., Tse, J. S., Tanaka, K., Marsiglio, F. & Ma, Y. Superconductivity in lithium under high pressure investigated with density functional and Eliashberg theory. *Phys. Rev. B* **79**, 054524 (2009).
 28. Rousseau, B. & Bergara, A. Giant anharmonicity suppresses superconductivity in AlH₃ under pressure. *Phys. Rev. B* **82**, 104504 (2011).
 29. Garland, J. W., Bennemann, K. H. & Mueller, F. M. Effect of Lattice Disorder on the Superconducting Transition Temperature. *Phys. Rev. Lett.* **21**, 1315 (1968).
 30. Lv, J., Wang, Y., Zhu, L. & Ma, Y. Predicted Novel High-Pressure Phases of Lithium. *Phys. Rev. Lett.* **106**, 015503 (2011).
 31. Li, P., Gao, G., Wang, Y. & Ma, Y. Crystal Structures and Exotic Behavior of Magnesium under Pressure. *J. Phys. Chem. C* **114**, 21745-21749 (2010).
 32. Zhu, L. *et al.* Substitutional Alloy of Bi and Te at High Pressure. *Phys. Rev. Lett.* **106**, 145501 (2011).
 33. Guillaume, C. L. *et al.* Cold melting and solid structures of dense lithium. *Nat. Phys.* **7**, 211-214 (2011).
 34. Perdew, J. P., Burke, K. & Ernzerhof, M. Generalized Gradient Approximation Made Simple. *Phys. Rev. Lett.* **77**, 3865 (1996).
 35. Kresse, G. & Furthmüller, J. Efficient iterative schemes for ab initio total-energy calculations using a plane-wave basis set. *Phys. Rev. B* **54**, 11169 (1996).
 36. Blöchl, P. E. Projector augmented-wave method. *Phys. Rev. B* **50**, 17953 (1994).
 37. Giannozzi, P. *et al.* QUANTUM ESPRESSO: a modular and open-source software project for quantum simulations of materials. *J. Phys.: Condens. Matter* **21**, 395502 (2009).

Acknowledgements

H. W. and Y. M. acknowledge Prof. Aitor Bergara for the valuable discussions and are thankful to the financial supports by Natural Science Foundation of China (NSFC) under No. 11104104, the China 973 Program (No. 2011CB808200), NSFC under Nos. 11025418 and 91022029, and the research fund of Key Laboratory of Surface Physics and Chemistry (No. SPC201103). T. I. was supported by MEXT of Japan (No. 20103001-20103005). The calculations were performed in the computing facilities at RICC system in RIKEN (Japan) and the High Performance Computing Center of Jilin University.

Author contributions

Y.M. proposed the concept. Y. M. and H. W. designed the simulations. H. W., J. T., K. T., Y.I., and Y. M. carried out the simulations and conducted the data analysis. H. W., J. T., and Y. M. wrote the manuscript.

*Correspondence and requests for materials should be addressed to Y.M.
(mym@jlu.edu.cn).

Figure captions

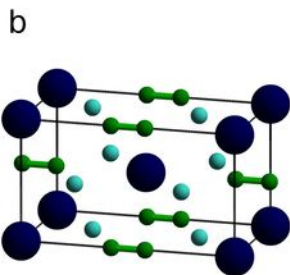
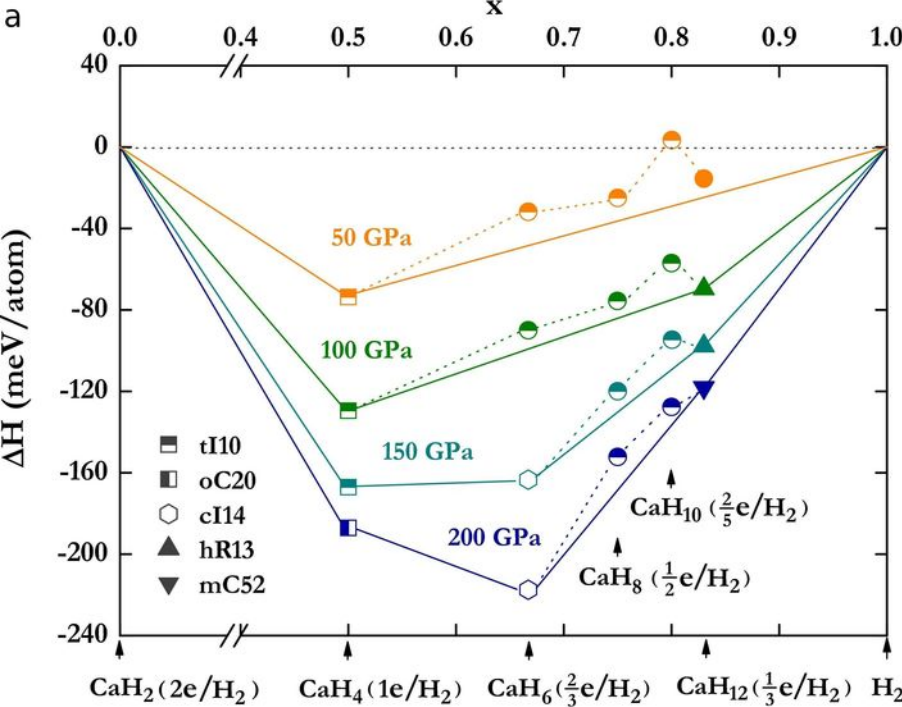
Figure 1 | Enthalpies of formation (ΔH , with respect to CaH_2 and H_2) of CaH_{2n} ($n=2-6$) and crystal structures. a. The abscissa x is the fraction of H_2 in the structures. The open, solid, and half-filled symbols indicate that the structures are composed of H_4 units, molecular H_2 , and the coexistence of H_2 and H , respectively. The metastable structures are indicated by circles. The stable pressure ranges for CaH_4 , CaH_6 , and CaH_{12} are 50–200 GPa, 150–200 GPa, and 100–200 GPa, respectively. The EAE (per H_2) is shown in brackets. The estimated stability fields were determined according to the static enthalpies and may shift upon inclusion of dynamic effects (the zero-point motion of the nuclei). **b.** Structure of tI10- CaH_4 . **c.** Structure of cI14- CaH_6 . **d.** Structure of hR13- CaH_{12} . Monatomic H , molecular H_2 , and Ca atoms are shown as cyan, green, and royal blue, respectively. The green cylinders and grey dashed lines are drawn to represent molecular H_2 and the sodalite cage, respectively.

Figure 2 | Hückel energy-level diagrams of H_4 and H_4^{2-} units. a. Hückel energy-level diagram of H_4 . **b.** Hückel energy-level diagram of H_4^{2-} . The partial occupation of electrons on the degenerate orbitals of H_4 units can lead to a Jahn–Teller distortion, but the H_4^{2-} possesses a closed shell electronic structure and therefore no Jahn–Teller distortion is expected.

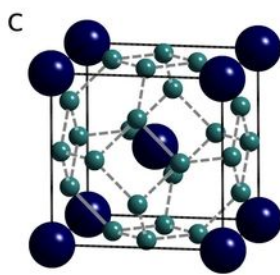
Figure 3 | Electron localization function (ELF) and band structure. a. ELF of CaH_0 (cI14 structure with H removed). **b.** ELF of CaH_6 . **c.** Band structure of CaH_6 . **d.** Band structure of Ca_0H_6 (cI14 structure with Ca removed). **e.** Band structure of CaH_0 . The horizontal dotted lines indicate the Fermi level.

Figure 4 | Phonon band structure and Eliashberg spectral function. Phonon dispersion curves of cI14 at 150 GPa (left panel). Olive circles indicate the phonon

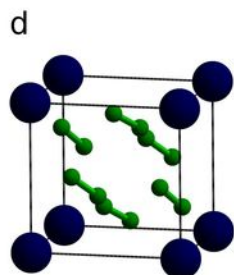
linewidth with a radius proportional to the strength. Phonons with a larger linewidth at Γ belong to the t_{2g} and e_g modes, as indicated by the circles at 960 cm^{-1} and 1960 cm^{-1} , respectively. Eliashberg electron-phonon coupling spectral function $\alpha^2F(\omega)$ at 150 GPa (right panel). Dashed line is the integration of the electron-phonon coupling strength as a function of phonon frequency. The horizon lines are drawn as a guide.



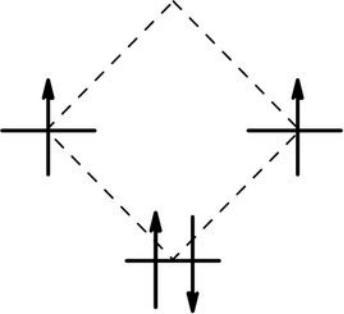
tI10



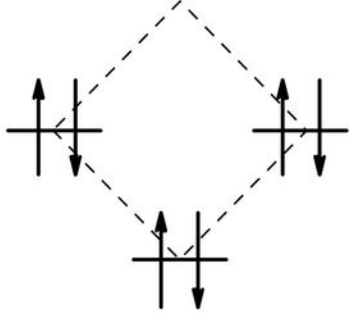
cI14



hR13



a



b

